Journal of Medicinal Chemistry

Article

pubs.acs.org/jmc

Discovery of a Phosphodiesterase 9A Inhibitor as a Potential Hypoglycemic Agent

Yong-xian Shao,[†,§,∥] Manna Huang,[‡,§,∥] Wenjun Cui,[§] Ling-Jun Feng,[†] Yinuo Wu,[†] Yinghong Cai,[†] Zhe Li,[†] Xinhai Zhu,[‡] Peiqing Liu,[†] Yiqian Wan,*[,‡] Hengming Ke,*[,§,†] and Hai-Bin Luo*[,†]

[†]School of Pharmaceutical Sciences, Sun Yat-Sen University, Guangzhou 510006, P. R. China

[‡]School of Chemistry and Chemical Engineering, Sun Yat-Sen University, Guangzhou 510275, P. R. China

[§]Department of Biochemistry and Biophysics and Lineberger Comprehensive Cancer Center, The University of North Carolina, Chapel Hill, North Carolina 27599-7260, United States

S *Supporting Information*

ABSTRACT: Phosphodiesterase 9 (PDE9) inhibitors have been studied as potential therapeutics for treatment of diabetes and Alzheimer's disease. Here we report a potent PDE9 inhibitor **3r** that has an IC_{50} of 0.6 nM and >150-fold selectivity over other PDEs. The HepG2 cell-based assay shows that **3r** inhibits the mRNA expression of phosphoenolpyruvate carboxykinase and glucose 6-phosphatase. These activities of **3r**, together with the reasonable pharmacokinetic properties and no acute toxicity at 1200 mg/kg dosage, suggest its potential as a hypoglycemic agent. The crystal structure of PDE9-**3r** reveals significantly different conformation and hydrogen bonding pattern of **3r** from those of previously published **28s**. Both **3r** and **28s** form a hydrogen bond with Tyr424, a unique PDE9 residue (except for PDE8), but **3r** shows an additional hydrogen bond with Ala452. This structure information might be useful for design of PDE9 inhibitors.

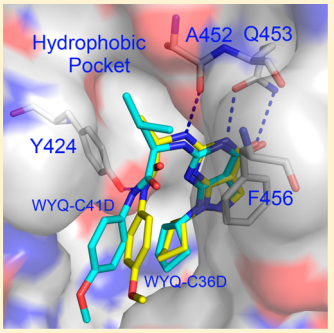

INTRODUCTION

Diabetes mellitus (DM) is a group of metabolic diseases that feature high blood sugar levels in patients. There are three main types of DM: type I or insulin-dependent DM in which the body fails to produce insulin; type II or insulin resistant DM in which there is dysregulation of insulin production/secretion as well as decreased sensitivity of peripheral tissues to insulin; and gestational diabetes that is typically associated with pregnant women.[1] DM affects 26 million Americans or 8.3% population in the United States (www.cdc.gov/diabetes/surveilance) and has become a worldwide threat to public health. Thus, discovery of hypoglycemic agents with strong potency and weak side effect is highly desirable.

Targeting at the signaling pathway of cyclic guanosine monophosphate (cGMP), which is a second messenger and plays critical roles in many physiological processes, appears to be a new promising direction to fight DM. An early study showed that the platelet cGMP concentration and the NO production were increased by insulin in dose-dependent manner.[2] Later, the NO/cGMP signaling pathway was shown to attenuate vascular inflammation and insulin resistance[3,4] and delay oocyte aging in DM.[5] Thus, regulation of cellular cGMP, which can be achieved via inhibition of phosphodiesterases (PDEs), would potentially be a strategy for treatment of DM. PDEs are a superfamily of enzymes that hydrolyze cGMP and cAMP and have been studied as drug targets for treatment of human diseases.[6−9] Twenty-one human PDE genes are classified into 11 families and encode >100 isoforms of proteins. PDE5, PDE6, and PDE9 specifically recognize cGMP as their substrate, while PDE4, PDE7, and PDE8 are cAMP-specific. The remaining PDE families are capable of degrading both cGMP and cAMP.[6−9]

The idea of targets at cGMP signaling pathway for treatment of DM originated from an early study that the cGMP-inhibited PDE (PDE3) played a critical role in the antilipolytic action of insulin.[10] Later, PDE3B was shown to mediate the inhibition of lipolysis by proinsulin C-peptide in diabetic rat adipose tissue[11] and to play an important role in acquisition of brown fat characteristics by white adipose tissue in male mice.[12] In addition, PDE5 inhibitors enhanced muscle microvascular blood flow and glucose uptake response to insulin[13] and improved dysfunction of metabolic and inflammatory processes in diabetic nephropathy.[14] Moreover, inhibition of PDE10A has been recently shown to protect mice from diet-induced obesity and insulin resistance.[15] For the highest affinity of cGMP with PDE9,[7] several PDE9 inhibitors were patented for the potential treatment of diabetes and cardiovascular diseases in early years.[16−20] After publication of the first PDE9 selective inhibitor BAY73-6691,[21] highly potent PDE9A inhibitors such as PF-04447943,[22] PF-4181366,[23] and **28s**[24] have been reported (Figure 1). However, interest in PDE9 inhibitors has shifted to their applications to CNS diseases such as Alzheimer's disease.[25−31] The most potent compound, PF-04447943, completed its phase II clinical trial for the treatment of mild Alzheimer's disease in April 2013.

Received: June 1, 2014
Published: November 28, 2014

   dx.doi.org/10.1021/jm500836h | *J. Med. Chem.* 2014, 57, 10304−10313

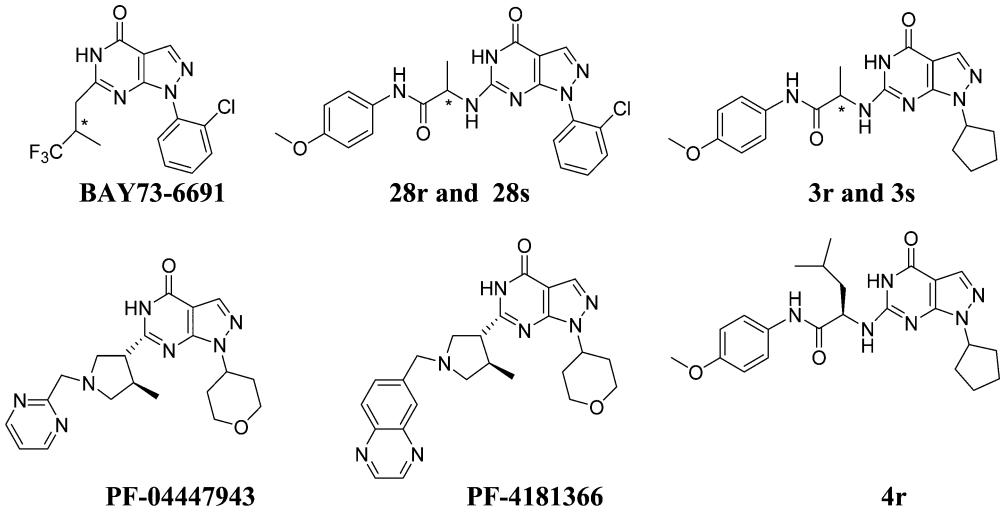

Figure 1. Chemical structures of PDE9 inhibitors. The symbol ∗ marks the chiral carbon that makes two enantiomers.

Scheme 1. Synthesis of PDE9A Inhibitors[a]

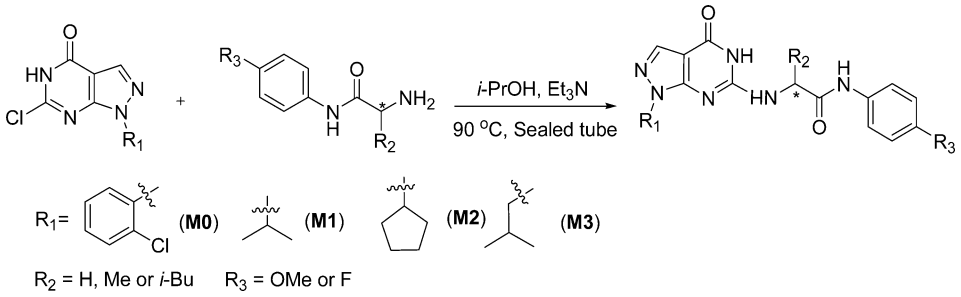

[a]Symbol ∗ marks the chiral carbon that makes two enantiomers.

Our initial effort on structure-based inhibitor design led to discovery of compound **28s** that uniquely forms a hydrogen bond with Tyr424 and has high affinity with PDE9A (IC_{50} = 21 nM) and good selectivity over other PDEs.[24] In this paper, we report an improved compound **3r** that has IC_{50} = 0.6 nM against PDE9A and at least 150-fold selectivity over other PDEs. The crystal structure of PDE9A-**3r** reveals significant differences in conformation and hydrogen bonding pattern between **3r** from **28s**. A cell-based assay shows that **3r** inhibits the mRNA expression of phosphoenolpyruvate carboxykinase (PEPCK) and glucose 6-phosphatase (G-6-Pase), implying its potential as a hypoglycemic agent.

RESULTS

Design of New PDE9A Inhibitors. We have previously reported a potent PDE9 inhibitor **28s** that has an IC_{50} of 21 nM against PDE9A and an 860-fold selectivity over PDE1B.[24] This compound directly forms a hydrogen bond with Tyr424 that is unique for PDE9 and PDE8 (phenylalanine in other PDE families) and may significantly contribute to selective binding of **28s** to PDE9 over other PDE families. However, since **28s** contains an L-Ala block (Figure 1) that is predicted to be sensitive to stomach proteases, its in vivo stability would be a potential problem. Thus, we chose the pyrazolopyrimidinone ring of **28s** as the scaffold and took the crystal structure of PDE9-**28s**[24] as the template to design new PDE9 inhibitors, in hopes of improvement on binding affinity and in vivo stability. Specifically, substitutions at the R_1 and R_3 positions and enantiomers at the R_2 position of **28s** (Scheme 1) were optimized to obtain stable and potent PDE9 inhibitors.

Structure–Activity Relationships. For the substitution at the R_1 position, the cyclopentyl group had better affinity for PDE9A than the isopropyl, isobutyl, or chlorophenyl group, as shown by the IC_{50} values of **3r** (0.6 nM), **6r** (1.0 nM), **7r** (17.6 nM), and **28r** (6.4 nM, Table 1). For the R_2 substitution, the methyl group was better than both hydrogen (**28r**/**28s** ∼ **1**, **3r**/**3s** ∼ **2**, **6r** ∼ **5**, Table 1) and the isobutyl group (**3r**/**3s** ∼ **4r**). The replacement of the methoxyl group with fluorine at the R_3 position produced similar affinity of the inhibitors against PDE9 (**3r** ∼ **8r**). Among the studied compounds, **3r** showed the best potency with an IC_{50} of 0.6 nM against the PDE9A catalytic domain (Table 1), which is 35-fold better than **28s**. This affinity improvement appears to be dominantly contributed by the replacement of chlorophenyl ring of **28s** with cyclopentyl group of **3r**.

The (*R*)-enantiomers of **28r** and **3r** showed 3- to 5-fold better affinity with PDE9 than their (*S*)-enantiomeric counterparts (Table 1). This result agrees with the early report that the (*R*)-enantiomer of BAY73-6691 has about 4-fold better affinity than its (*S*)-enantiomer.[32] Explanation of this consistency is not clear, but it might mean that the binding pocket of PDE9 has a special shape for better fitting of the (*R*)-enantiomers than the (*S*)-enantiomers.

To investigate (*R*)-/(*S*)-enantiomers' impact on selectivity, inhibitions of both (*R*)-/(*S*)-enantiomers of **3** and **28** were assayed against other PDE families (Table 2). Overall, all four compounds of **3** and **28** predominantly inhibit PDE9 with

dx.doi.org/10.1021/jm500836h | J. Med. Chem. 2014, 57, 10304−10313

Table 1. Chemical Structures of Inhibitors and Their Affinities (IC_{50}) with PDE9A2 (181−506)[a]

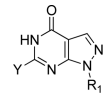

Compounds	Y	R_1	IC_{50} ± SD (nM)	Predicted Ki (nM)[#]
1	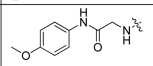		52.0 ± 8.1	40
28r	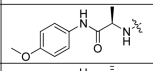		6.4 ± 1.5	5.0
28s*	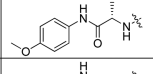		21 ± 5	16
2	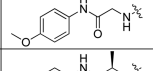		5.5 ± 0.6	4.3
3r	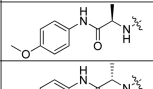		0.60 ± 0.02	0.5
3s	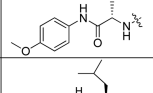		3.0 ± 0.8	2.3
4r	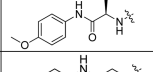		8.1 ± 1.3	6.3
5	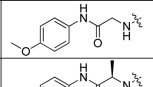		25.9 ± 3.7	20.0
6r	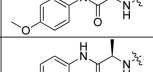		1.05 ± 0.03	0.8
7r	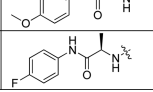		17.6 ± 1.6	13.6
8r	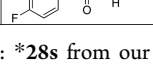		1.1 ± 0.2	0.9

[a]Footnotes: ***28s*** from our previous report.[24] [#]The predicted K_i was calculated with equation $IC_{50} = K_i(1 + [S]/K_M)$, where [S] = 20 nM and K_M = 70 nM were used.

moderate selectivity over PDE5A1 (22- to 150-fold, Table 2). (*R*)-Enantiomers of **3r** and **28r** showed better affinity than their (*S*)-enantiomers against PDE1B2, PDE5A1, PDE7A1, and PDE10A2, but no consistent trend was observed for PDE4D2 (Table 2). Both enantiomers of **3** and **28** barely inhibit PDE8 (IC_{50} of ∼100 μM, Table 2), which also contains a tyrosine at the corresponding position of Tyr424 of PDE9A2, implying that the inhibitory selectivity is jointly determined by multiple residues at the active sites of the PDE families.

We further tested the impact of the substitutions and enantiomers on the plasma protein binding (PPB) to see how much of the inhibitors are freely available for their binding to PDE9. The PPB assay was conducted using human plasma for compounds **3r**, **3s**, and **28s** at concentrations of 1 and 5 μM (Supporting Information S1). In short, these compounds strongly interact with plasma proteins, as shown by the bound percentage of >94.3%. The enantiomers and substitutions at the R_1 position do not significantly impact the binding of these compounds to plasma proteins. Although a large percentile for plasma protein binding implies reduced availability of inhibitors for their targets,[34] remaining free **3r** in blood plasma might be sufficient for blocking the PDE9-cGMP signaling because of its high affinity with PDE9 (IC_{50} of 0.6 nM).

Binding of 3r to PDE9. The X-ray structure of PDE9-**3r**, which was prepared by soaking of the PDE9-IBMX crystal in 2 mM **3r**, shows definite **3r** binding to the active site of PDE9A2 (Figure 2). The electron density in ($2F_o - F_c$) and ($F_o - F_c$) maps clearly revealed the unique conformation of **3r**. The pyrazolopyrimidinone ring of **3r** forms two hydrogen

Table 2. IC_{50} (nM) of PDE9 Inhibitors

PDE catalytic domain	PDE9A2 (181−506)	PDE1B2 (10−487)	PDE4D2 (86−413)	PDE5A1 (535−860)	PDE7A1 (130−482)	PDE8A1 (480−820)	PDE10A2 (448−789)	PDE2A3 (222−904)	PDE3A (679−1087)
3r	0.60 ± 0.02	473 ± 14 (788)[a]	21200 ± 700 (35333)	90.6 ± 23 (151)	1800 ± 700 (3067)	>100000	6900 ± 100 (11567)	13000 ± 240 (21666)	33200 ± 3250 (55000)
3s	3.0 ± 0.8	2300 ± 200 (750)	1400 ± 200 (476)	417 ± 24 (139)	17900 ± 3200 (5967)	>100000	33300 ± 1200 (11100)		
28r	6.4 ± 1.5	1900 ± 700 (294)	13600 ± 3100 (2123)	141 ± 22 (22.0)	51200 ± 8200 (7981)	>100000	3700 ± 140 (570)		
28s	21 ± 5	18000 ± 1600 (857)	15700 ± 2400 (748)	3300 ± 500 (157)	>100000	>100000	>50000	>50000	>50000

[a]The numbers in parentheses are the fold of inhibitory selectivity of PDE9 over other PDEs.

dx.doi.org/10.1021/jm500836h | J. Med. Chem. 2014, 57, 10304−10313

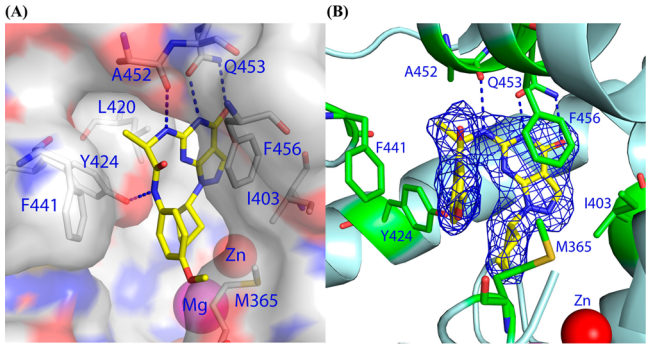

Figure 2. Binding of **3r** to PDE9A. (A) Surface presentation of the **3r** binding to the active site pocket of PDE9A2. Atoms of carbon, nitrogen, and oxygen of PDE9A are presented in colors of white, blue, and red, respectively. Inhibitor **3r** is shown as yellow sticks. Dotted lines represent hydrogen bonds. (B) Ribbon model of the **3r** binding. The blue mesh is the electron density of the difference ($F_o - F_c$) map that was calculated from the structure with omission of **3r** and contoured at 3σ.

bonds with invariant Gln453 and aromatic π-stack against Phe456, which are two characteristic interactions of inhibitors with various PDE families,[33] in addition to the hydrophobic contacts with Leu420 and Ala452. The cyclopentyl ring of **3r** orients toward the metal binding pocket and closely contacts Met365 and Tyr424. The tail of **3r** (*N*-(4-methoxyphenyl)-2-(methylamino)propanamide) forms two hydrogen bonds, respectively, with the side chain of Tyr424 and the carbonyl oxygen of Ala452 (Figure 2), in addition to the hydrophobic interactions with Met365, Leu420, Phe441, Ala452, and Phe456.

Inhibitor **3r** has a binding pattern overall similar to that of **28s** (Figure 3), as seen from the superimposable pyrazolopyrimidinone rings and similar location of their remaining groups.

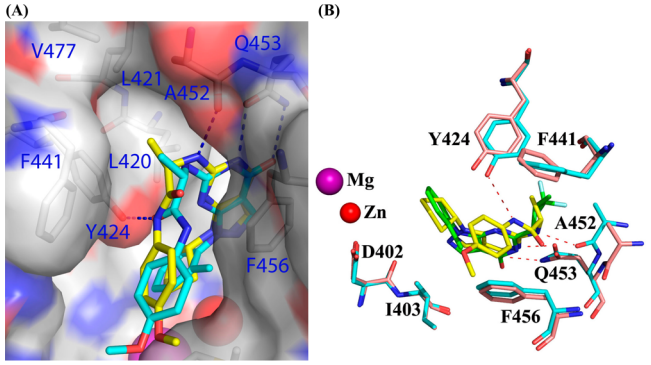

Figure 3. Comparison on binding of several PDE9 inhibitors. (A) Superposition between the crystal structures of PDE9-**3r** (yellow sticks) and PDE9-**28s** (cyan). PDE9 is presented in the surface mode. (B) Superposition between the crystal structures of PDE9-**3r** (cyan and yellow sticks) and PDE9-(R)-BAY73-6691 (salmon and green sticks).

However, the tails of **3r** and **28s** show significantly different conformations and interactions (Figure 3), although they have the similar chemical components and occupy the same locations. The replacement of the L-Ala block of **28s** by a D-Ala unit of **3r** causes significant changes of hydrogen-bonding pattern. Tyr424 forms a hydrogen bond with the amide oxygen of L-Ala of **28s** in the structure of PDE9-**28s**[24] but switches to the nitrogen adjacent to D-Ala of **3r** (Figure 3A). Interestingly, the nitrogen atom of D-Ala of **3r** forms a hydrogen bond (2.9 Å) with the carbonyl oxygen of Ala452, in contrast to the very weak contact (4.0 Å) in the PDE9-**28s** structure. This difference in hydrogen bond pattern might explain the 35-fold better affinity of **3r** than **28s**.

Significant Improvement of the in Vivo Properties of 3r over 28s. A preliminary pharmacokinetic analysis revealed that **3r** has C_{max} of 217 ng/mL, bioavailability of 9.8%, and $T_{1/2}$ of 1.7 h in the oral administration mode (Table 3). These parameters show a significant improvement over these of **28s** (C_{max} of 16 ng/mL, $T_{1/2}$ of 0.3 h, and bioavailability of 1.3%). The pharmacokinetic parameters of **3r** from the intravenous administration, such as C_0 = 24 mg/L and $T_{1/2}$ =5.3 h (Table 3), appear to be promising, but further studies are required for usability of **3r** in intravenous administration mode. On the other hand, **8r** shows reasonable pharmacokinetic properties of 18% bioavailability and $T_{1/2}$ of 4.1 h in the oral administration mode (Table 3).

To further characterize properties of the compounds, solubility of **3r**, **3s**, and **28s** was measured in simulated gastric/intestinal fluids. All the three compounds were more soluble in the simulated intestinal fluid (31, 31, and 13 μg/mL at pH 6.8 for **3r**, **3s**, and **28s**) than in the simulated gastric fluid (26, 23, and 8 μg/mL at pH 1.4, Table 4). Comparable solubility of **3r** and **3s**

Table 4. Solubility Comparisons of PDE9 Inhibitors in Simulated Gastric/Intestinal Fluids

	solubility ± SD (μg/mL, N = 4)		
simulated fluids	**3r**	**3s**	**28s**
gastric fluid (pH 1.4)	26 ± 7	23 ± 5	8 ± 2
intestinal fluid (pH 6.8)	31 ± 4	31 ± 8	13 ± 3

in the simulated gastric and intestinal fluids implies no strong effect of the chirality on the solubility. However, the replacement of the chloral-phenyl group of **28s** by the cyclic pentanyl ring of **3r** (Figure 1), which is the only chemical difference between **3r**/**3s** and **28s**, appears to significantly contribute to the solubility.

The solubility data imply that the moderate 9.8% bioavailability of **3r** may be due to its metabolic instability. Thus, we test the **3r** stability in the mouse liver microsomes. The results showed that **3r** was not very stable in the mouse liver microsome, as shown by $T_{1/2}$ of 23 min and E_h of 73% (Table 5). However, **3r** is significantly better than the positive control

Table 3. Pharmacokinetic Profile of PDE9A Inhibitors 3r and 8r in Mice/Rats[a]

route iv	CL (L h^{-1} kg^{-1})	V_{ss} (L/kg)	MRT$_{(0-\infty)}$ (h)	AUC$_{0-t}$ (mg·h/L)	AUC$_{0-\infty}$ (mg·h/L)	C_0 (μg/L)	$T_{1/2}$ (h)	T_{max} (h)
3r	1.43 ± 0.23	1.53 ± 0.15	1.08 ± 0.08	3529 ± 575	3550 ± 590	24535 ± 7525	5.34 ± 1.43	
8r	1.78 ± 0.18	2.58 ± 0.07	0.59 ± 0.13	2821 ± 268	2825 ± 270	19085 ± 428	1.01 ± 0.09	
route po	CL (L h^{-1} kg^{-1})	V_{ss} (L/kg)	MRT$_{(0-\infty)}$ (h)	AUC$_{0-t}$ (mg·h/L)	AUC$_{0-\infty}$ (mg·h/L)	C_{max} (μg/L)	$T_{1/2}$ (h)	T_{max} (h)	F (%)
3r	14.6 ± 3.5	35.0 ± 7.9	2.65 ± 0.82	346 ± 111	360 ± 101	217 ± 30	1.67 ± 0.04	0.58 ± 0.38	9.8 ± 3.1
8r			3.94 ± 1.11	463 ± 153	520 ± 213	135 ± 55	4.08 ± 1.00	1.00 ± 0.87	18 ± 7

[a]Dose: 5 mg/kg. po = oral administration. iv = intravenous administration.

dx.doi.org/10.1021/jm500836h | J. Med. Chem. 2014, 57, 10304−10313

Table 5. Metabolic Stability of 3r in Liver Microsomes of CD-1 Mouse[a]

compd	k	$T_{1/2}$ (min)	Cl_{int} (mL min^{-1} mg^{-1})	Cl_{app} (mL min^{-1} kg^{-1})	Cl_h (mL min^{-1} kg^{-1})	E_h (%)
testosterone	0.34604	2.0	0.6921	2725.1	87.1	96.8
propranolol	0.45726	1.5	0.9145	3600.9	87.8	97.6
warfarin	0.00393	176.5	0.0079	30.9	23.0	25.6
3r	0.03102	22.3	0.0620	244.3	65.8	73.1

[a]Testosterone, propranolol, and warfarin are the positive controls.

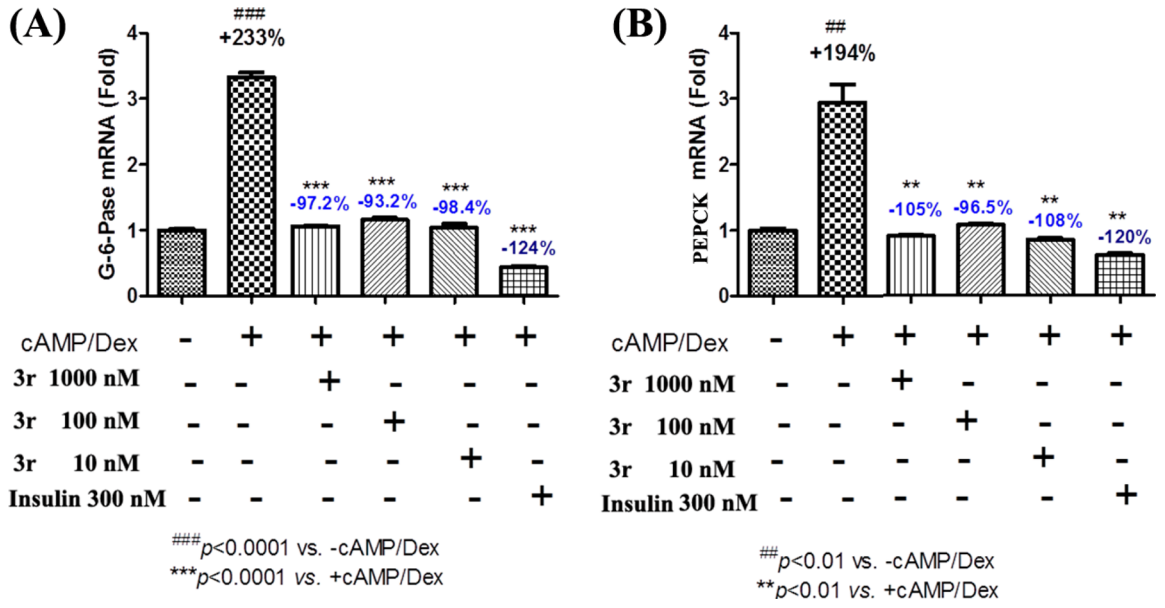

Figure 4. Inhibition of the mRNA expression in HepG2 cell line by PDE9 inhibitor **3r**: (A) G-6-Pase mRNA expression; (B) PEPCK mRNA expression.

compounds of testosterone and propranolol, which have $T_{1/2}$ of ~2 min and E_h of ~97% (Table 5).

Inhibitor 3r Does Not Show Acute Toxicity. Compound **3r** was evaluated for acute toxicity. Twenty-four mice were randomly divided into three groups and given in single oral doses of 0, 600, or 1200 mg/kg **3r** on the first day. The animals treated with **3r** did not show any poisoned symptoms and mortality immediately or during the post-treatment period of 2 weeks. In addition, no abnormal behaviors and significant changes of water/food consumption and body weight were observed during the period of the experiments. Therefore, **3r** was well tolerated up to a dose of 1200 mg/kg and has no acute toxicity.

Inhibition on mRNA Expression of PEPCK and G-6-Pase in HepG2 Cell by 3r. Upon stimulation by 8-Br-cAMP/dexamethasone, the mRNA expression of two key hepatic gluconeogenic genes of the HepG2 cell, PEPCK and G-6-Pase, was enhanced respectively by 233% and 194% relative to the basal level of the mRNA expression (Figure 4). As a positive control, 300 nM insulin reduced the mRNA expression of PEPCK and G-6-Pase to the basal level in HepG2 cell in the presence of stimulation of cAMP/dexamethasone. As shown in Figure 4, **3r** at 10 nM sufficiently reduced the 8-Br-cAMP/dexamethasone-induced expression of PEPCK and G-6-Pase back to the basal level in HepG2 cells, implying that our inhibitor **3r** is a potential hypoglucemic agent.

DISCUSSION

Hints for Improvement of PDE9 Inhibitors. Compound **28s** effectively inhibits PDE9 at enzymatic level, but its in vivo stability needs to be improved. Although the cause of instability is not clear, three weak chemical links in **28s** are possibly the candidates: the amide bond of the L-Ala unit, the methoxyl group, and the N-link between nitrogen and pyrazolopyrimidinone (Figure 1). The L-Ala unit appears to be mostly unstable and would be easily hydrolyzed by stomach proteases. Because D-amino acids are in general more stable than L-amino acids in stomach, the replacement of L-Ala with D-Ala may be a major factor for the prolonged $T_{1/2}$ values (0.85, 1.7, and 4.1 h for **28s**, **3r**, and **8r** in the oral administration mode and 0.32, 5.34, and 1.01 h for **28s**, **3r**, and **8r** in the intravenous administration mode, Table 3 and unpublished data for **28s**). The longer $T_{1/2}$ value of **8r** (4.1 h) than **3r** (1.7 h) in the po mode might imply slower absorption of **8r** by intestinal. However, the shorter $T_{1/2}$ value of **8r** (~1 h) than **3r** (~5 h) in the iv mode might imply that **8r** is unstable and decomposable in liver. In short, the explanation of the data of metabolic stability and bioavailability could not be firmly concluded, and further improvement of the compounds is desirable.

The crystal structure of PDE9-**3r** shows that the methyl side chain of D-Ala of **3r** points toward a hydrophobic subpocket that is composed of Leu420, Leu421, Phe441, Ala452, and Val457 (Figure 3A). Thus, a tentative modification on the inhibitors might be an extension of the side chain of D-Ala with hydrophobic groups such as propanyl chain to fill the hydrophobic pocket for improvement of affinity and selectivity. This extension might also serve as a stereo-obstacle to protect the N-link and amide bond of the compounds from decomposition in vivo by live enzymes. Following this assumption, compound **4r** that contains D-isoleucine in the place of D-Ala of **3r** was synthesized.

dx.doi.org/10.1021/jm500836h | J. Med. Chem. 2014, 57, 10304−10313

Unfortunately, the enzymatic assay shows slightly reduced potency of **4r** (IC_{50} = 8.1 nM) in comparison to 0.6 nM of **3r**. A molecular docking suggests that **4r** binds to PDE9 in a similar pattern to **3r** with slight position shift of the whole molecule, but the side chain of D-Leu did not penetrate into the small hydrophobic pocket. It remains to be elucidated if D-Leu could serve as a stereo-obstacle so as to improve the in vivo stability and if other replacements such as a straight propanyl group could penetrate the hydrophobic pocket and thus improve the affinity and stability.

CONCLUSION

Our structure-based design led to discovery of a PDE9 selective inhibitor **3r** that is capable of inhibiting the mRNA expression of PEPCK and F-6-Pase and thus a potential hypoglucemic agent.

EXPERIMENTAL SECTION

Molecular Docking. Hydrogen atoms and charges were added to the PDE9A structure (PDB entry code 4GH6)[24] using the CHARMM force field and the Momany−Rone partial charge method as implemented in Accelrys Discovery Studio 2.5.5.[35] All ionizable residues in the systems were set to their protonation states at a neutral pH. The zinc and magnesium ions were assigned with a charge of +2. Ligand **28s** was used to define the active site of PDE9A and test docking by the CDOCKER[36] and LigandFit[37] protocols embedded in Accelrys Discovery Studio 2.5.5. The radius of the input sphere was set as 10 Å from the center of the binding site, and the rest of the docking parameters used the default values. Fifty random conformations were generated and optimized for each ligand. The output poses from docking were evaluated by the score of the program and also by visual inspection.

Syntheses. ^{1}H NMR and ^{13}C NMR spectra were recorded at room temperature on a Mercury-Plus 300 instrument or a Bruker AVANCE III 400 instrument with TMS as an internal reference. LC/MS was run on a LCMS-2010A. Thin-layer chromatography was performed on precoated silica gel F-254 plates (0.25 mm, E. Merck). Element analyses were carried out with a Vario EL series analyzer. Melting points were determined on a WRS-1B digital melting point apparatus and were not calibrated. IR spectra were recorded on a Thermo 330 FT-IR. All starting materials and reagents were purchased from commercial suppliers and used directly without further purification.

The syntheses of **M0** and **28s** were previously reported.[24] Syntheses of intermediates **M1**−**M3** and compounds **28r** and **1**−**8r** are shortly described as follows. The pyrazolopyrimidinones (**M1**−**M3**) and 2-amino-*N*-phenylacetamide derivatives with R_2 and R_3 substitutions (Scheme 1) were synthesized by the similar protocols in literature.[24,38] Briefly, to a 10 mL of sealed vial were added *i*-PrOH (3 mL), pyrazolopyrimidinones (0.5 mmol), 2-amino-*N*-phenylacetamide derivatives (1.0 mmol), and Et_3N (1.5 mmol). The reaction mixture was stirred in an oil bath preheated to 90 °C. After completion of the reaction as indicated by TLC, the reaction mixture was cooled to room temperature and concentrated in vacuo. The residue was purified by flash column chromatography on silica gel (eluted with DCM/MeOH = 25:1) to provide the targeted compounds. The following are the characterization of the compounds. The data of elemental analysis for all the new compounds are provided in the Supporting Information S2.

*6-Chloro-1-isopropyl-1H-pyrazolo[3,4-d]pyrimidin-4-ol (**M1**).* White solid, yield, 80%. Mp: 216−217 °C. MS (ESI$^-$), *m*/*z*: 211 ([M − H]$^-$). ^{1}H NMR (400 MHz, $CDCl_3$) δ (ppm) 8.12 (s, 1H), 5.01 (hept, *J* = 6.7 Hz, 1H), 1.54 (d, *J* = 6.7 Hz, 6H). ^{13}C NMR (101 MHz, $CDCl_3$) δ (ppm) 159.9, 150.7, 145.7, 1345.0, 104.1, 49.8, 22.0. IR (KBr, cm^{-1}): 3434, 3085, 2976, 2877, 1715, 1674, 1585, 1526, 1442, 1268, 1119, 957, 884, 778, 686, 557, 467. Purity >99.5%.

*6-Chloro-1-cyclopentyl-1H-pyrazolo[3,4-d]pyrimidin-4-ol (**M2**).* White solid, yield, 82%. Mp: 228−230 °C. MS (ESI$^-$), *m*/*z*: 237 ([M − H]$^-$). ^{1}H NMR (400 MHz, $CDCl_3$) δ (ppm) 8.10 (s, 1H), 5.15 (p, *J* = 7.5 Hz, 1H), 2.20−2.04 (m, 4H), 2.02−1.91 (m, 2H), 1.72 (ddd, *J* = 11.2, 7.8, 3.2 Hz, 2H). ^{13}C NMR (101 MHz, $CDCl_3$) δ (ppm) 159.9, 151.4, 145.8, 135.1, 104.3, 58.4, 32.6, 24.8. IR (KBr, cm^{-1}): 3429, 2951, 2871, 1713, 1674, 1583, 1529, 1444, 1273, 1227, 1089, 957, 883, 778, 675, 553. Purity >99.5%.

*6-Chloro-1-isobutyl-1H-pyrazolo[3,4-d]pyrimidin-4-ol (**M3**).* White solid, yield, 70%. Mp: 146−148 °C. MS (ESI$^-$), *m*/*z*: 225 ([M − H]$^-$). ^{1}H NMR (400 MHz, $CDCl_3$) δ (ppm) 12.45 (brs, 1H), 8.11 (s, 1H), 4.13 (d, *J* = 7.4 Hz, 2H), 2.33 (dp, *J* = 13.8, 6.9 Hz, 1H), 0.92 (d, *J* = 6.7 Hz, 6H). ^{13}C NMR (101 MHz, $CDCl_3$) δ (ppm) 159.9, 152.0, 146.0, 135.1, 103.9, 54.9, 29.0, 19.8. IR (KBr, cm^{-1}): 3424, 3094, 3070, 3013, 2958, 2873, 1714, 1673, 1582, 1534, 1448, 1393, 1273, 1230, 1204, 1171, 1157, 1076, 1033, 957, 886, 778, 743, 672, 547. Purity >99.5%.

*(R)-2-((1-(2-Chlorophenyl)-4-hydroxy-1H-pyrazolo[3,4-d]-pyrimidin-6-yl)amino)-N-(4-methoxyphenyl)propanamide (**28r**).* White solid, yield, 60%. Mp: 155−156 °C. MS (ESI$^-$), *m*/*z*: 437 ([M − H]$^-$). ^{1}H NMR (300 MHz, $CDCl_3$) δ (ppm) 10.59 (brs, 1H), 8.17 (brs, 1H), 8.12 (s, 1H), 7.53−7.45 (m, 2H), 7.41−7.29 (m, 2H), 7.09 (d, *J* = 8.9 Hz, 2H), 7.00 (d, *J* = 5.0 Hz, 1H), 6.77 (d, *J* = 8.9 Hz, 2H), 4.50 (p, *J* = 6.8 Hz, 1H), 3.76 (s, 3H), 1.49 (d, *J* = 6.9 Hz, 3H). ^{13}C NMR (75 MHz, $CDCl_3$) δ (ppm) 170.9, 159.6, 156.8, 155.4, 153.1, 137.0, 135.5, 131.9, 130.6, 130.4, 129.7, 127.6, 122.1, 114.2, 100.9, 55.8, 51.7, 17.9. IR (pure, cm^{-1}): 3292, 3072, 2933, 2835, 1678, 1602, 1509, 1548, 1509, 1490, 1237, 1117, 1033, 971, 828, 672. Purity >99.5%.

*2-((1-(2-Chlorophenyl)-4-hydroxy-1H-pyrazolo[3,4-d]pyrimidin-6-yl)amino)-N-(4-methoxyphenyl)acetamide (**1**).* White solid, yield, 50%. Mp 213-215 °C. MS (ESI$^-$), *m*/*z*: 423 ([M − H]$^-$). ^{1}H NMR (400 MHz, DMSO-d_6) δ (ppm) 10.87 (brs, 1H), 9.93 (s, 1H), 8.05 (s, 1H), 7.66−7.62 (m, 1H), 7.55−7.49 (m, 2H), 7.47−7.38 (m, 3H), 7.01 (brs, 1H), 6.92−6.85 (m, 2H), 3.98 (d, *J* = 4.7 Hz, 2H), 3.72 (s, 3H). ^{13}C NMR (101 MHz, DMSO-d_6) δ (ppm) 166.9, 158.1, 156.0, 155.8, 154.3, 136.7, 135.9, 132.3, 131.4, 131.0, 130.7, 130.3, 128.3, 121.2, 114.4, 100.5, 55.6, 44.5. IR (pure, cm^{-1}): 3268, 3101, 2837, 1678, 1613, 1543, 1511, 1488, 1445, 1413, 1393, 1300, 1242, 1061, 1030, 965, 828, 763, 673, 639. Purity >99.5%.

*2-((1-Cyclopentyl-4-hydroxy-1H-pyrazolo[3,4-d]pyrimidin-6-yl)-amino)-N-(4-methoxyphenyl)acetamide (**2**).* White solid, yield, 50%. Mp:220−221 °C. MS (ESI$^-$), *m*/*z*: 381 ([M − H]$^-$). ^{1}H NMR (400 MHz, DMSO-d_6) δ (ppm) 10.02 (s, 1H), 7.76 (s, 1H), 7.50 (d, *J* = 9.0 Hz, 2H), 6.92−6.84 (m, 3H), 4.89 (p, *J* = 7.4 Hz, 1H), 4.13 (d, *J* = 5.1 Hz, 2H), 3.72 (s, 3H), 1.99−1.87 (m, 4H), 1.87−1.75 (m, 2H), 1.65−1.52 (m, 2H). ^{13}C NMR (101 MHz, DMSO-d_6) δ (ppm) 167.4, 158.2, 155.8, 153.9, 153.6, 134.3, 132.4, 121.2, 114.4, 100.3, 57.2, 55.6, 44.7, 32.0, 24.6. IR (pure, cm^{-1}): 3457, 3274, 3068, 2967, 1683, 1665, 1608, 1528, 1514, 1314, 1245, 1171, 1052, 1032, 823, 776, 726, 707, 628. Purity >99.5%.

*(R)-2-((1-Cyclopentyl-4-hydroxy-1H-pyrazolo[3,4-d]pyrimidin-6-yl)amino)-N-(4-methoxyphenyl)propanamide (**3r**).* White solid, yield, 23%. Mp: 135−136 °C. MS (ESI$^-$), *m*/*z*: 395 ([M − H]$^-$). ^{1}H NMR (400 MHz, $CDCl_3$) δ (ppm) 7.74 (s, 1H), 7.47 (d, *J* = 9.0 Hz, 2H), 6.86 (d, *J* = 9.1 Hz, 2H), 4.86−4.77 (m, 1H), 4.46 (q, *J* = 6.9 Hz, 1H), 3.68 (s, 3H), 1.92 (dd, *J* = 8.4, 5.0 Hz, 2H), 1.75 (t, *J* = 7.2 Hz, 4H), 1.62−1.45 (m, 2H), 1.40 (d, *J* = 7.0 Hz, 3H). ^{13}C NMR (101 MHz, $CDCl_3$) δ (ppm) 174.9, 161.9, 159.4, 157.3, 156.1, 137.9, 135.7, 124.8, 117.8, 103.8, 61.0, 59.2, 54.6, 35.4, 35.2, 28.0, 28.0, 22.1. IR (pure, cm^{-1}): 3299, 2952, 2871, 1675, 1605, 1547, 1510, 1444, 1238, 1034, 827, 775. Purity >99.5%.

*(S)-2-((1-Cyclopentyl-4-hydroxy-1H-pyrazolo[3,4-d]pyrimidin-6-yl)amino)-N-(4-methoxyphenyl)propanamide (**3s**).* White solid, yield, 34%. Mp:133−134 °C. MS (ESI$^-$), *m*/*z*: 395 ([M − H]$^-$). ^{1}H NMR (400 MHz, DMSO-d_6) δ (ppm) 10.44 (s, 1H), 10.08 (s, 1H), 7.75 (s, 1H), 7.55−7.49 (m, 2H), 6.93−6.86 (m, 3H), 4.88 (p, *J* = 7.3 Hz, 1H), 4.56 (p, *J* = 6.8 Hz, 1H), 3.72 (s, 3H), 2.02−1.92 (m, 2H), 1.88−1.77 (m, 4H), 1.63−1.51 (m, 2H), 1.44 (d, *J* = 6.9 Hz, 3H). ^{13}C NMR (101 MHz, DMSO-d_6) δ (ppm) 171.1, 158.1, 155.8, 153.8, 152.8, 134.3, 132.4, 121.3, 114.3, 100.4, 57.3, 55.6, 50.9, 32.0, 31.9, 24.6, 24.5, 19.1. IR (pure, cm^{-1}): 3301, 2959, 1675, 1605, 1548, 1510, 1448, 1238, 1035, 827, 775. Purity >99.5%.

*(R)-2-((1-Cyclopentyl-4-oxo-4,5-dihydro-1H-pyrazolo[3,4-d]-pyrimidin-6-yl)amino)-N-(4-methoxyphenyl)-4-methylpentanamide (**4r**).* White solid, yield, 52%. Mp: 118−120 °C. MS (ESI$^-$), *m*/*z*: 439 ([M + H]$^+$). ^{1}H NMR (400 MHz, $CDCl_3$) δ (ppm) 10.67 (s, 1H), 8.65 (s, 1H), 7.77 (s, 1H), 7.39 (d, *J* = 6.3 Hz, 2H), 6.77 (d, *J* = 6.8 Hz, 2H), 4.90 (s, 1H), 4.64 (s, 1H), 3.71 (s, 3H), 2.12−1.48 (m, 11H), 0.91 (s, 6H). ^{13}C NMR (101 MHz, $CDCl_3$) δ (ppm) 171.0, 160.0, 156.7, 153.5, 152.4, 134.4, 130.4, 122.0, 114.1, 100.1, 57.5, 55.4, 54.4, 41.2, 32.0, 24.9, 24.6, 22.9, 22.0. IR (KBr, cm^{-1}): 3328, 2955, 1679, 1609, 1551, 1511, 1448, 1242, 1170, 1037, 882, 778, 707. Purity >99.5%.

*2-((4-Hydroxy-1-isopropyl-1H-pyrazolo[3,4-d]pyrimidin-6-yl)-amino)-N-(4-methoxyphenyl)acetamide (**5**).* White solid, yield, 35%. Mp: 178−179 °C. MS (ESI$^-$), *m*/*z*: 355 ([M − H]$^-$). ^{1}H NMR (400 MHz, DMSO-d_6) δ (ppm) 10.72 (s, 1H), 10.02 (s, 1H), 7.75 (s, 1H), 7.49 (d, *J* = 9.0 Hz, 2H), 6.88 m, 3H), 4.78−4.67 (m, 1H), 4.14 (d, *J* = 5.1 Hz, 2H), 3.72 (s, 3H), 1.36 (d, *J* = 6.7 Hz, 6H). ^{13}C NMR (101 MHz, DMSO-d_6) δ (ppm) 167.4, 158.2, 155.8, 153.6, 153.4, 134.2, 132.3, 121.3, 114.4, 100.4, 55.6, 48.4, 44.7, 22.0. IR (pure, cm^{-1}): 3308, 2979, 1675, 1608, 1542, 1510, 1497, 1444, 1414, 1246, 1034, 826, 778. Purity >99.5%.

*(R)-2-((4-Hydroxy-1-isopropyl-1H-pyrazolo[3,4-d]pyrimidin-6-yl)-amino)-N-(4-methoxyphenyl)propanamide (**6r**).* White solid, yield, 54%. Mp: 131−132 °C. MS (ESI$^-$), *m*/*z*: 369 ([M − H]$^-$). ^{1}H NMR (400 MHz, $CDCl_3$) δ (ppm) 7.87 (s, 1H), 7.41 (d, *J* = 8.9 Hz, 2H), 6.83 (d, *J* = 8.9 Hz, 2H), 4.85−4.78 (m, 2H), 4.70−4.62 (m, 1H), 3.77 (s, 3H), 1.58 (d, *J* = 7.0 Hz, 3H), 1.45 (dd, *J* = 14.9, 6.7 Hz, 6H). ^{13}C NMR (101 MHz, $CDCl_3$) δ (ppm) 171.0, 159.9, 156.8, 153.0, 152.0, 134.5, 130.3, 121.9, 114.2, 100.3, 55.4, 51.5, 48.9, 21.8, 17.8. IR (pure, cm^{-1}): 3284, 2980, 2937, 1678, 1605, 1546, 1510, 1443, 1239, 1135, 1033, 828, 776. Purity >99.5%.

*(R)-2-((4-Hydroxy-1-isobutyl-1H-pyrazolo[3,4-d]pyrimidin-6-yl)-amino)-N-(4-methoxyphenyl)propanamide (**7r**).* White solid, yield, 40%. Mp: 146−147 °C. MS (ESI$^-$), *m*/*z*: 383 ([M − H]$^-$). ^{1}H NMR (400 MHz, $CDCl_3$) δ (ppm) 7.75 (s, 1H), 7.51−7.44 (m, 2H), 6.88−6.82 (m, 2H), 4.47 (q, *J* = 6.9 Hz, 1H), 3.92−3.74 (m, 2H), 3.68 (s, 3H), 2.05 (dp, *J* = 13.6, 6.8 Hz, 1H), 1.40 (d, *J* = 7.0 Hz, 3H), 0.69 (d, *J* = 6.7 Hz, 3H), 0.63 (d, *J* = 6.7 Hz, 3H). ^{13}C NMR (101 MHz, $CDCl_3$) δ (ppm) 174.9, 162.0, 159.4, 158.1, 156.3, 138.1, 135.8, 124.8, 117.8, 103.4, 59.2, 57.2, 54.5, 32.3, 23.6, 23.5, 22.2. IR (pure, cm^{-1}): 3305, 2960, 1678, 1608, 1548, 1510, 1448, 1414, 1240, 1171, 1033, 827, 776, 758, 726, 698, 640. Purity >99.5%.

*(R)-2-((1-Cyclopentyl-4-oxo-4,5-dihydro-1H-pyrazolo[3,4-d]-pyrimidin-6-yl)amino)-N-(4-fluorophenyl)propanamide (**8r**).* White solid, yield, 57%. Mp: 223−224 °C. MS (ESI$^-$), *m*/*z*: 385 ([M + H]$^+$). ^{1}H NMR (400 MHz, DMSO-d_6) δ (ppm) 10.43 (s, 1H), 10.29 (s, 1H), 7.75 (s, 1H), 7.69−7.55 (m, 2H), 7.16 (t, *J* = 8.9 Hz, 2H), 6.92 (d, *J* = 6.5 Hz, 1H), 4.92−4.79 (m, 1H), 4.54 (p, *J* = 6.7 Hz, 1H), 2.02−1.90 (m, 2H), 1.80 (t, *J* = 7.6 Hz, 4H), 1.64−1.48 (m, 2H), 1.44 (d, *J* = 6.9 Hz, 3H). ^{13}C NMR (101 MHz, DMSO-d_6) δ (ppm) 171.5, 158.0, 157.3, 153.7, 152.7, 135.7, 134.3, 121.4, 121.3, 115.8, 115.6, 100.3, 57.3, 51.0, 31.9, 31.8, 24.5, 24.4, 18.9. IR (pure, cm^{-1}): 3425, 2961, 2872, 2027, 1677, 1611, 1554, 1510, 1448, 1409, 1297, 1264, 1218, 1153, 1098, 1077, 1043, 1004, 952, 909, 833, 779, 690, 616, 571. Purity >99.5%.

Protein Expression and Purification. The PDE9A2 catalytic domain (residues 181−506) was subcloned to vector pET15b and purified according to the protocols described previously.[39,40] Briefly, the pET15-PDE9 plasmid was transferred into *E. coli* strain BL21 (Codonplus, Stratagene) for overexpression. When the *E. coli* cell was grown in LB medium at 37 °C to absorption A_{600} = 0.7, 0.1 mM isopropyl β-D-thiogalactopyranoside was added to induce the expression at 15 °C overnight. Recombinant PDE9A2 protein was purified by column chromatography of Ni-NTA, Q-Sepharose, and Superdex-200 (GE Healthcare). A typical batch of purification yielded 20−60 mg of PDE9A2 from a liter cell culture. The PDE9A2 proteins had purity greater than 95% as judged by mini SDS−PAGE, in which no visible bands for other proteins were visible when >20 μg of PDE protein was loaded into the GEL. The catalytic domains of PDE5A1 (535−860), PDE4D2 (86−413), PDE7A1 (130−482), PDE8A2 (480−820), and PDE10A2 (448−789) were purified by the published protocols.[41−45] PDE1B (10−516) was expressed and purified using a similar protocol.

Enzymatic Assay. The enzymatic activities of PDEs were assayed by using ^{3}H-cGMP or ^{3}H-cAMP as the substrate. The assay buffer was 50 mM Tris-HCl, pH 8.0, 10 mM $MgCl_2$ or 4 mM $MnCl_2$, 1 mM DTT, and 20 nM ^{3}H-cGMP or ^{3}H-cAMP (20 000−30 000 cpm/assay, GE Healthcare). The reaction was carried out at room temperature for 15 min and then terminated by addition of 0.2 M $ZnSO_4$. The reaction product ^{3}H-GMP was precipitated by adding 0.2 N $Ba(OH)_2$, while the unreacted ^{3}H-cGMP remained in the supernatant. Radioactivity in the supernatant was measured in 2.5 mL of Ultima Gold liquid scintillation cocktails by a liquid scintillation counter. For the measurement of IC_{50}, at least eight concentrations of inhibitors were used in the presence of suitable substrates. The enzymes used in the assay had about final 50−200 ng/mL concentration and hydrolyzed up to 70% of the substrates. Each measurement was repeated three times. The IC_{50} values were calculated by nonlinear regression.

Crystallization and Structure Determination. The crystals of PDE9A2 were grown by using hanging drop vapor diffusion method. The PDE9A2 (181−506) (8−10 mg/mL) in a buffer of 50 mM NaCl, 20 mM Tris-HCl, pH 7.5, 1 mM β-mercaptoethanol, and 1 mM EDTA was mixed with 2 mM IBMX overnight before setting-up of crystallization against the well buffer of 0.1 M HEPES (pH 7.5), 3.0 M sodium formate at 4 °C. Crystals of the PDE9-**3r** complex were prepared by soaking the PDE9-IBMX cocrystals in the crystallization buffer plus 2 mM **3r** at 25 °C for 3 days. The crystals were flash-frozen in liquid nitrogen by using the well buffer plus 20% glycerol as the cryosolvent. X-ray diffraction data were collected at λ = 1.075 on beamline X29 in Brookhaven National Laboratory and processed by HKL 2000 (Table 6).[46] The structure of the PDE9-**3r** complex was solved by the molecular replacement, using the PDE9A2 catalytic domain of the PDE9-IBMX complex as the initial model.[39] The resulting model was rebuilt by program O[47] and refined by CNS (Table 6).[48]

Table 6. Statistics on Diffraction Data and Structure Refinement

parameter	PDE9-**3r**
space group	$P4_12_12$
unit cell: *a*, *c* (Å)	103.6, 268.7
resolution (Å)	2.0
total measurements	953,981
unique reflections	91 112
completeness (%)	91.5 (71.8)[a]
average I/σ	23.0 (3.1)[a]
R_{merge}	0.065 (0.258)[a]
Structure Refinement	
R-factor	0.241
R_{free}	0.268
resolution (Å)	30.0−2.0
reflections	91 068 (9098)[b]
rms deviation for	
bond length (Å)	0.006
bond angle (deg)	1.2
average *B*-factor (Å^2)	
protein	36.8 (5306)[c]
inhibitor **3r**	31.2 (58)[c]
Zn	40.0 (2)[c]
Mg	28.6 (2)[c]
water	36.8 (299)[c]

[a]The numbers in parentheses are for the highest resolution shell. [b]The number of reflections omitted for calculation of R_{free}. [c]The number of atoms in the crystallographic asymmetric unit.

Cell-Based Assay for Inhibition on the mRNA Expression of PEPCK and G-6-Pase. The cell-based assay was performed following the protocols described in literature.[49] HepG2 cells were incubated in

serum at 37 °C in 5% CO_2 overnight and then grown in the absence of serum for starvation overnight. After starvation, 1 μM dexamethasone (20 mM stock in 100% DMSO) and 0.5 mM 8-Br-cAMP (100 mM stock in water) were added and further incubated for 30 h. Various concentrations of PDE9 inhibitor **3r** were then added into the culture medium and incubated for 12 h. The mRNAs were extracted from the treated HepG2 cell with Ultrapure RNA kit. The genes of G-6-Pase and PEPCK were instantly synthesized by addition of 100 ng of cDNA and detected by qPCR.

Pharmacokinetics Analysis. Pharmacokinetic properties of **3r** and **8r** were analyzed by HDBioscieces and Medicilon Companies, Shanghai, China. Fifteen male CD-1 mice that are 5 weeks old and have body weight of 17−20 g (Shanghai Laboratory Animal Center, China) were used for the pharmacokinetic experiments of **3r**. Six male SD rats with body weight of 230−260 g were purchased from Shanghai SIPPR-BK LAB Animal Ltd., Shanghai, China, and used for the pharmacokinetic analysis of **8r**. Compound **3r** was dissolved/suspended in 5% DMSO, 10% Cremophor, and 85% saline for intravenous administration (iv) and in 5% DMSO and 95% (26% SBE-β-CD) for oral administration (po). Compounds **28s** and **8r** were formulated in 10% DMSO plus 40% HP-β-CD and 5% DMSO/95% (20% HP-β-CD) for the po and iv administrations. A final dosage of 5 mg/kg mouse/rat of the formulated compounds was administrated, and the blood samples were taken at various time points in 24 h. The concentration of the compounds in blood was analyzed by LC−MS/MS (Shimadzu liquid chromatographic system and API4000 mass spectrometer, Applied Biosystems, Ontario, Canada).

Solubility of PDE9A Inhibitors in Simulated Gastric/Intestinal Fluids. The simulated gastric fluid was prepared by dissolving 1 g of pepsin (Aladdin) into diluted hydrochloric acid, pH 1.4. The simulated intestinal fluid was prepared by dissolving 1 g of trypsin (Aladdin) into a solution of KH_2PO_4, pH 6.8. Compounds **3r**, **3s**, and **28s** were dissolved in acetonitrile (HPLC-grade, Honeywell Burdick & Jackson) and mixed with the internal standard 1,3-dimethyl-5-fluorouracil (Sigma) to generate the standard curve.

The excess compounds **3r**, **3s**, and **28s** were incubated with the simulated gastric/intestinal fluids (4 mL) for 24−48 h at 37 °C. After 24−48 h, the samples were passed through 0.22 μm filter (Millipore) and then loaded to the HPLC system. HPLC experiments were performed in a Shimadzu LC-20AT HPLC system, and wavelength of 254 nm was used for detection. A Thermo Hypersil MOS-2 C_8 column (150 mm × 4.6 mm, 5 mm) was run at 37 °C with a mobile phase of 0.1% aqueous formic acid and 0.1% formic acid acetonitrile (60:40%, v/v) at flow rate of 1.0 mL/min. The retention time and peak area were determined for each compound. The average peak areas from the triplicate measurements were compared with the standard curve to calculate the mean solubility.

Stability of 3r in the Mouse Liver Microsome. CD-1 mouse liver microsome was purchased from BD Gentest Corporation (Woburn, MA, USA). Compound **3r** was dissolved in 100% DMSO as 10 mM stock solution and diluted to a final concentration of 0.5 μM for the experiments. Warfarin (Sigma, St. Louis, MO, USA), testosterone (Acros, Belgium), and propranolol (TRC, Toronto, Canada) were used as the positive controls. Liver microsome incubations were conducted in duplicate in 96-well plates. Each well contains 30 μL of 0.1 M potassium phosphate buffer (pH 7.4), 3.0 mM $MgCl_2$, 0.75 mg/mL mouse liver microsome, and 0.75 μM **3r** or the positive controls. After 5 min of preincubation at 37 °C, 15 μL of 3 mM NADPH in 0.1 M potassium phosphate buffer was added to initiate the enzymatic reaction. Reactions were terminated at various time points (0, 5, 10, 20, 30 min) by adding 90 μL of ice-cold acetonitrile containing internal standard. A parallel incubation was performed using 0.1 M potassium phosphate buffer (pH 7.4) as the negative control, and reactions were terminated after 30 min incubation. A Shimadzu liquid chromatographic system and an API4000 mass spectrometer equipped with Turbo Ion Spray (ESI) interface (Applied Biosystems, Concord, Ontario, Canada) were used for detection. Analyst 1.5 software packages (Applied Biosystems) were used for control of the LC−MS/MS system, as well as data acquisition and processing.

Acute Toxicity of 3r. The acute toxicity was tested following the similar protocols described in our previous study.[50] Twenty-four KM mice (22 days, 18−20 g), purchased from the Laboratory Animal Center of Sun Yat-Sen University (Guangzhou, China), were used to evaluate the acute toxicity of **3r**. Mice were randomly divided into three groups, each of which was given in single oral dose of 0, 600, or 1200 mg/kg **3r** on the first day of the experiment. Mice were maintained on a 12 h light/dark cycle (light from 7:00 to 19:00) at room temperature and 60−70% relative humidity. Sterile food and water were given according to the institutional guidelines. Prior to each experiment, mice were fasted overnight and allowed free access to water. Compound **3r** was dissolved in 5% DMSO and 95% (26% SBE-β-CD) solution and orally administrated. Mice were observed for any abnormal behavior and mortality and weighed at the fourth hour of **3r** administration and then every 24 h for 14 days. Animals were sacrificed on the 14th day, and tissue samples of heart, liver, and kidney were macroscopically examined for possible damages.

■ ASSOCIATED CONTENT

Ⓢ Supporting Information

Plasma protein binding and elements analysis results of PDE9A inhibitors. This material is available free of charge via the Internet at http://pubs.acs.org.

Accession Codes

The atomic coordinates and structure factors have been deposited into the RCSB Protein Data Bank with accession number 4QGE.

■ AUTHOR INFORMATION

Corresponding Authors

*Y.W.: phone, 86-20-84113610; e-mail, ceswyq@mail.sysu.edu.cn.
*H.K.: phone, 1-919-966-2244; e-mail, hke@med.unc.edu.
*H.-B.L.: phone, 86-20-39943031; e-mail, luohb77@mail.sysu.edu.cn.

Author Contributions

‖Y.-x.S. and M.H. contributed equally.

Notes

The authors declare no competing financial interest.

■ ACKNOWLEDGMENTS

This work is partially supported by U.S. NIH Grant GM59791 (H.K.), National High Technology Research and Development Program of China (863 Program, No. 2006AA09Z446), Natural Science Foundation of China (Grants 21272287, 21272282, 21103234, and 81373258), Research Fund for the Doctoral Program of Higher Education of China (Grant 20130171110096), and Guangdong Natural Science Foundation (Grants S2011030003190 and S2013010014867). We thank Dr. Yuehong Xu who kindly provided the simulated gastric/intestinal fluids.

■ ABBREVIATIONS USED

PDE, phosphodiesterase; cGMP, cyclic guanosine monophosphate; cAMP, cyclic adenosine monophosphate; DM, diabetes mellitus; PEPCK, phosphoenolpyruvate carboxykinase; G-6-Pase, glucose 6-phosphatase

■ REFERENCES

(1) National Diabetes Data Group. Classification and diagnosis of diabetes mellitus and other categories of glucose intolerance. *Diabetes* **1979**, *28*, 1039−1057.

(2) Anfossi, G.; Mularoni, E. M.; Burzacca, S.; Ponziani, M. C.; Massucco, P.; Mattiello, L.; Cavalot, F.; Trovati, M. Platelet resistance to nitrates in obesity and obese NIDDM, and normal platelet

sensitivity to both insulin and nitrates in lean NIDDM. *Diabetes Care* **1998**, *21*, 121−126.
(3) Rizzo, N. O.; Maloney, E.; Pham, M.; Luttrell, I.; Wessells, H.; Tateya, S.; Daum, G.; Handa, P.; Schwartz, M. W.; Kim, F. Reduced NO-cGMP signaling contributes to vascular inflammation and insulin resistance induced by high-fat feeding. *Arterioscler., Thromb., Vasc. Biol.* **2010**, *30*, 758−765.
(4) Tateya, S.; Rizzo, N. O.; Handa, P.; Cheng, A. M.; Morgan-Stevenson, V.; Daum, G.; Clowes, A. W.; Morton, G. J.; Schwartz, M. W.; Kim, F. Endothelial NO/cGMP/VASP signaling attenuates Kupffer cell activation and hepatic insulin resistance induced by high-fat feeding. *Diabetes* **2011**, *60*, 2792−2801.
(5) Goud, A. P.; Goud, P. T.; Diamond, M. P.; Gonik, B.; Abu-Soud, H. M. Activation of the cGMP signaling pathway is essential in delaying oocyte aging in diabetes mellitus. *Biochemistry* **2006**, *45*, 11366−11378.
(6) Maurice, D. H.; Ke, H.; Ahmad, F.; Wang, Y.; Chung, J.; Manganiello, V. C. Advances in targeting cyclic nucleotide phosphodiesterases. *Nat. Rev. Drug Discovery* **2014**, *13*, 290−314.
(7) Conti, M.; Beavo, J. Biochemistry and physiology of cyclic nucleotide phosphodiesterases: essential components in cyclic nucleotide signaling. *Annu. Rev. Biochem.* **2007**, *76*, 481−511.
(8) Omori, K.; Kotera, J. Overview of PDEs and their regulation. *Circ. Res.* **2007**, *100*, 309−327.
(9) Ke, H.; Wang, H.; Ye, M. Structural insight into the substrate specificity of phosphodiesterases. *Handb. Exp. Pharmacol.* **2011**, *204*, 121−134.
(10) Degerman, E.; Belfrage, P.; Manganiello, V. C. Structure, localization, and regulation of cGMP-inhibited phosphodiesterase (PDE3). *J. Biol. Chem.* **1997**, *272*, 6823−6826.
(11) Guirguis, E.; Hockman, S.; Chung, Y. W.; Ahmad, F.; Gavrilova, O.; Raghavachari, N.; Yang, Y.; Niu, G.; Chen, X.; Yu, Z. X.; Liu, S.; Degerman, E.; Manganiello, V. A role for phosphodiesterase 3B in acquisition of brown fat characteristics by white adipose tissue in male mice. *Endocrinology.* **2013**, *154*, 3152−3167.
(12) Ghorbani, A.; Omrani, G. R.; Hadjzadeh, M. A.; Varedi, M. Proinsulin C-peptide inhibits lipolysis in diabetic rat adipose tissue through phosphodiestrase-3B enzyme. *Horm. Metab Res.* **2013**, *45*, 221−225.
(13) Genders, A. J.; Bradley, E. A.; Rattigan, S.; Richards, S. M. cGMP phosphodiesterase inhibition improves the vascular and metabolic actions of insulin in skeletal muscle. *Am. J. Physiol. Endocrinol. Metab.* **2011**, *301*, E342−E350.
(14) Thompson, C. S. Diabetic nephropathy: Treatment with phosphodiesterase type 5 inhibitors. *World J. Diabetes* **2013**, *4*, 124−129.
(15) Nawrocki, A. R.; Rodriguez, C. G.; Toolan, D. M.; Price, O.; Henry, M.; Forrest, G.; Szeto, D.; Keohane, C. A.; Pan, Y.; Smith, K. M.; Raheem, I. T.; Cox, C. D.; Hwa, J.; Renger, J. J.; Smith, S. M. Genetic deletion and pharmacological inhibition of phosphodiesterase 10A protects mice from diet-induced obesity and insulin resistance. *Diabetes* **2014**, *63*, 300−311.
(16) Fryburg, D. A.; et al. Treatment of insulin resistance syndrome and type 2 diabetes with PDE9 inhibitors. WO 03/037432 A1, 2003.
(17) Deninno, M. P.; et al. PDE9 inhibitors for treating cardiovascular disorders. WO 03/037899, 2003; Pfizer Inc.
(18) Bell, A. S.; et al. PDE9 inhibitors for treating type 2 diabetes, metabolic syndrome, and cardiovasculate disease. WO 2004/096811, 2004.
(19) Black, S. C.; Gibbs, E. M.; McNeish, J. D. Phosphodiesterase 9 inhibition as treatment for obesity-related conditions. WO 2005/041972, 2005.
(20) Deninno, M. P.; Andrews, M.; Bell, A. S.; Chen, Y.; Eller-Zarbo, C.; Eshelby, N.; Etienne, J. B.; Moore, D. E.; Palmer, M. J.; Visser, M. S.; Yu, L. J.; Zavadoski, W. J.; Michael Gibbs, E. The discovery of potent, selective, and orally bioavailable PDE9 inhibitors as potential hypoglycemic agents. *Bioorg. Med. Chem. Lett.* **2009**, *19*, 2537−2541.
(21) Wunder, F.; Tersteegen, A.; Rebmann, A.; Erb, C.; Fahrig, T.; Hendrix, M. Characterization of the first potent and selective PDE9 inhibitor using a cGMP reporter cell line. *Mol. Pharmacol.* **2005**, *68*, 1775−1781.
(22) Verhoest, P. R.; Fonseca, K. R.; Hou, X.; Proulx-Lafrance, C.; Corman, M.; Helal, C. J.; Claffey, M. M.; Tuttle, J. B.; Coffman, K. J.; Liu, S.; Nelson, F.; Kleiman, R. J.; Menniti, F. S.; Schmidt, C. J.; Vanase-Frawley, M.; Liras, S. Design and discovery of 6-[(3*S*,4*S*)-4-methyl-1-(pyrimidin-2-ylmethyl)pyrrolidin-3-yl]-1-(tetrahydro-2*H*-pyran-4-yl)-1,5-dihydro-4*H*-pyrazolo[3,4-*d*]pyrimidin-4-one (PF-04447943), a selective brain penetrant PDE9A inhibitor for the treatment of cognitive disorders. *J. Med. Chem.* **2012**, *55*, 9045−9054.
(23) Verhoest, P. R.; Proulx-Lafrance, C.; Corman, M.; Chenard, L.; Helal, C. J.; Hou, X.; Kleiman, R.; Liu, S.; Marr, E.; Menniti, F. S.; Schmidt, C. J.; Vanase-Frawley, M.; Schmidt, A. W.; Williams, R. D.; Nelson, F. R.; Fonseca, K. R.; Liras, S. Identification of a brain penetrant PDE9A inhibitor utilizing prospective design and chemical enablement as a rapid lead optimization strategy. *J. Med. Chem.* **2009**, *52*, 7946−7949.
(24) Meng, F.; Hou, J.; Shao, Y. X.; Wu, P. Y.; Huang, M.; Zhu, X.; Cai, Y.; Li, Z.; Xu, J.; Liu, P.; Luo, H.-B.; Wan, Y.; Ke, H. Structure-based discovery of highly selective phosphodiesterase-9A inhibitors and implications for inhibitor design. *J. Med. Chem.* **2012**, *55*, 8549−8558.
(25) van der Staay, F. J.; Rutten, K.; Bärfacker, L.; Devry, J.; Erb, C.; Heckroth, H.; Karthaus, D.; Tersteegen, A.; van Kampen, M.; Blokland, A.; Prickaerts, J.; Reymann, K. G.; Schröder, U. H.; Hendrix, M. The novel selective PDE9 inhibitor BAY 73-6691 improves learning and memory in rodents. *Neuropharmacology* **2008**, *55*, 908−918.
(26) Hutson, P. H.; Finger, E. N.; Magliaro, B. C.; Smith, S. M.; Converso, A.; Sanderson, P. E.; Mullins, D.; Hyde, L. A.; Eschle, B. K.; Turnbull, Z.; Sloan, H.; Guzzi, M.; Zhang, X.; Wang, A.; Rindgen, D.; Mazzola, R.; Vivian, J. A.; Eddins, D.; Uslaner, J. M.; Bednar, R.; Gambone, C.; Le-Mair, W.; Marino, M. J.; Sachs, N.; Xu, G.; Parmentier-Batteur, S. The selective phosphodiesterase 9 (PDE9) inhibitor PF-04447943(6-[(3*S*,4*S*)-4-methyl-1-(pyrimidin-2-ylmethyl)pyrrolidin-3-yl]-1-(tetrahydro-2*H*-pyran-4-yl)-1,5-dihydro-4*H*-pyrazolo[3,4-*d*]pyrimidin-4-one) enhances synaptic plasticity and cognitive function in rodents. *Neuropharmacology* **2011**, *61*, 665−676.
(27) Vardigan, J. D.; Converso, A.; Hutson, P. H.; Uslaner, J. M. The selective phosphodiesterase 9 (PDE9) inhibitor PF-04447943 attenuates a scopolamine-induced deficit in a novel rodent attention task. *J. Neurogenet.* **2011**, *25*, 120−126.
(28) Liddie, S.; Anderson, K.; Paz, A.; Itzhak, Y. The effect of phosphodiesterase inhibitors on extinction of cocaine-induced conditioned place preference in mice. *J. Psychopharmacol.* **2012**, *26*, 1375−1382.
(29) Kroker, K. S.; Rast, G.; Giovannini, R.; Marti, A.; Dorner-Ciossek, C.; Rosenbrock, H. Inhibition of acetylcholinesterase and phosphodiesterase-9A has differential effects on hippocampal early and late LTP. *Neuropharmacology* **2012**, *62*, 1964−1974.
(30) Kleiman, R. J.; Chapin, D. S.; Christoffersen, C.; Freeman, J.; Fonseca, K. R.; Geoghegan, K. F.; Grimwood, S.; Guanowsky, V.; Hajós, M.; Harms, J. F.; Helal, C. J.; Hoffmann, W. E.; Kocan, G. P.; Majchrzak, M. J.; McGinnis, D.; McLean, S.; Menniti, F. S.; Nelson, F.; Roof, R.; Schmidt, A. W.; Seymour, P. A.; Stephenson, D. T.; Tingley, F. D.; Vanase-Frawley, M.; Verhoest, P. R.; Schmidt, C. J. Phosphodiesterase 9A regulates central cGMP and modulates responses to cholinergic and monoaminergic perturbation in vivo. *J. Pharmacol. Exp. Ther.* **2012**, *341*, 396−409.
(31) Claffey, M. M.; Helal, C. J.; Verhoest, P. R.; Kang, Z.; Fors, K. S.; Jung, S.; Zhong, J.; Bundesmann, M. W.; Hou, X.; Lui, S.; Kleiman, R. J.; Vanase-Frawley, M.; Schmidt, A. W.; Menniti, F.; Schmidt, C. J.; Hoffman, W. E.; Hajos, M.; McDowell, L.; O'Connor, R. E.; Macdougall-Murphy, M.; Fonseca, K. R.; Becker, S. L.; Nelson, F. R.; Liras, S. Application of structure-based drug design and parallel chemistry to identify selective, brain penetrant, in vivo active phosphodiesterase 9A inhibitors. *J. Med. Chem.* **2012**, *55*, 9055−9068.

(32) Wang, H.; Luo, X.; Ye, M.; Hou, J.; Robinson, H.; Ke, H. Insight into binding of phosphodiesterase-9A selective inhibitors by crystal structures and mutagenesis. *J. Med. Chem.* **2010**, *53*, 1726−1731.
(33) Ke, H.; Wang, H. Crystal structures of phosphodiesterases and implications on substrate specificity and inhibitor selectivity. *Curr. Top. Med. Chem.* **2007**, *7*, 391−403.
(34) Stephen, H. C.; Robin, W. *Drug Disposition and Pharmacokinetics: From Principles to Applications*; John Wiley & Sons, Ltd.: Hoboken, NJ, 2011.
(35) *Accelrys Discovery Studio*, version 2.5.5; Accelrys Software Inc.: San Diego, CA, 2010.
(36) Wu, G.; Robertson, D. H.; Brooks, C. L.; Vieth, M. Detailed analysis of grid-based molecular docking: a case study of CDOCKER—A CHARMm-based MD docking algorithm. *J. Comput. Chem.* **2003**, *24*, 1549−1562.
(37) Venkatachalam, C. M.; Jiang, X.; Oldfield, T.; Waldman, M. LigandFit: a novel method for the shape-directed rapid docking of ligands to protein active sites. *J. Mol. Graphics Modell.* **2003**, *21*, 289−307.
(38) Gilbert, A. M.; Nowak, P.; Brooijmans, N.; Bursavich, M. G.; Dehnhardt, C.; Santos, E. D.; Feldberg, L. R.; Hollander, I.; Kim, S.; Lombardi, S.; Park, K.; Venkatesan, A. M.; Mallon, R. Novel purine and pyrazolo[3,4-*d*]pyrimidine inhibitors of PI3 kinase-alpha: hit to lead studies. *Bioorg. Med. Chem. Lett.* **2010**, *20*, 636−639.
(39) Huai, Q.; Wang, H.; Zhang, W.; Colman, R. W.; Robinson, H.; Ke, H. Crystal structure of phosphodiesterase 9 shows orientation variation of inhibitor 3-isobutyl-1-methylxanthine binding. *Proc. Natl. Acad. Sci. U.S.A.* **2004**, *101*, 9624−9629.
(40) Hou, J.; Xu, J.; Liu, M.; Zhao, R.; Luo, H.-B.; Ke, H. Structural asymmetry of phosphodiesterase-9, potential protonation of a glutamic acid, and role of the invariant glutamine. *PLoS One* **2011**, *6*, e18092.
(41) Wang, H.; Liu, Y.; Huai, Q.; Cai, J.; Zoraghi, R.; Francis, S. H.; Corbin, J. D.; Robinson, H.; Xin, Z.; Lin, G.; Ke, H. Multiple conformations of phosphodiesterase-5: implications for enzyme function and drug development. *J. Biol. Chem.* **2006**, *281*, 21469−21479.
(42) Wang, H.; Liu, Y.; Chen, Y.; Robinson, H.; Ke, H. Multiple elements jointly determine inhibitor selectivity of cyclic nucleotide phosphodiesterases 4 and 7. *J. Biol. Chem.* **2005**, *280*, 30949−30955.
(43) Wang, H.; Yan, Z.; Yang, S.; Cai, J.; Robinson, H.; Ke, H. Kinetic and structural studies of phosphodiesterase-8A and implication on the inhibitor selectivity. *Biochemistry* **2008**, *47*, 12760−12768.
(44) Wang, H.; Liu, Y.; Hou, J.; Zheng, M.; Robinson, H.; Ke, H. Structural insight into substrate specificity of phosphodiesterase 10. *Proc. Natl. Acad. Sci. U.S.A.* **2007**, *104*, 5782−5787.
(45) Huai, Q.; Wang, H.; Sun, Y.; Kim, H. Y.; Liu, Y.; Ke, H. Three-dimensional structures of PDE4D in complex with roliprams and implication on inhibitor selectivity. *Structure* **2003**, *11*, 865−873.
(46) Otwinowski, Z.; Minor, W. Processing of X-ray diffraction data collected in oscillation mode. *Methods Enzymol.* **1997**, *276*, 307−326.
(47) Jones, T. A.; Zou, J.-Y.; Cowan, S. W.; Kjeldgaard, M. Improved methods for building protein models in electron density maps and the location of errors in these models. *Acta Crystallogr.* **1991**, *A47*, 110−119.
(48) Brünger, A. T.; Adams, P. D.; Clore, G. M.; DeLano, W. L.; Gros, P.; Grosse-Kunstleve, R. W.; Jiang, J. S.; Kuszewski, J.; Nilges, M.; Pannu, N. S.; Read, R. J.; Rice, L. M.; Simonson, T.; Warren, G. L. Crystallography and NMR system: a new software suite for macromolecular structure determination. *Acta Crystallogr.* **1998**, *D54*, 905−921.
(49) Kim, Y. D.; Park, K. G.; Lee, Y. S.; Park, Y. Y.; Kim, D. K.; Nedumaran, B.; Jang, W. G.; Cho, W. J.; Ha, J.; Lee, I. K.; Lee, C. H.; Choi, H. S. Metformin inhibits hepatic gluconeogenesis through AMP-activated protein kinase-dependent regulation of the orphan nuclear receptor SHP. *Diabetes* **2008**, *57*, 306−314.
(50) Luo, Z.; Sheng, J.; Sun, Y.; Lu, C.; Yan, J.; Liu, A.; Luo, H.-B.; Huang, L.; Li, X. Synthesis and evaluation of multi-target-directed ligands against Alzheimer's disease based on the fusion of donepezil and ebselen. *J. Med. Chem.* **2013**, *56*, 9089−9099.